Photosensitive gold-nanoparticle-embedded dielectric nanowires

MING-SHIEN HU[1,2], HSIN-LI CHEN[3,4], CHING-HSING SHEN[4], LU-SHENG HONG[1], BOHR-RAN HUANG[3], KUEI-HSIEN CHEN[2,4] AND LI-CHYONG CHEN[4]*

[1]Department of Chemical Engineering, National Taiwan University of Science and Technology, Taipei 106, Taiwan
[2]Institute of Atomic and Molecular Sciences, Academia Sinica, Taipei 106, Taiwan
[3]Department and Institute of Electronic Engineering, National Yunlin University of Science and Technology, Yunlin 640, Taiwan
[4]Center for Condensed Matter Sciences, National Taiwan University, Taipei 106, Taiwan
*e-mail: chenlc@ccms.ntu.edu.tw

Published online: 22 January 2006; doi:10.1038/nmat1564

Noble-metal nanoparticles embedded in dielectric matrices are considered to have practical applications in ultrafast all-optical switching devices owing to their enhanced third-order nonlinear susceptibility, especially near the surface-plasmon-resonance (SPR) frequency[1,2]. Here we present the use of a microreactor approach to the fabrication of a self-organized photosensitive gold nanoparticle chain encapsulated in a dielectric nanowire. Such a hybrid nanowire shows pronounced SPR absorption. More remarkably, a strong wavelength-dependent and reversible photoresponse has been demonstrated in a two-terminal device using an ensemble of gold nanopeapodded silica nanowires under light illumination, whereas no photoresponse was observed for the plain silica nanowires. These results show the potential of using gold nanopeapodded silica nanowires as wavelength-controlled optical nanoswitches. The microreactor approach can be applied to the preparation of a range of hybrid metal–dielectric one-dimensional nanostructures that can be used as functional building blocks for nanoscale waveguiding devices, sensors and optoelectronics.

Noble-metal nanoparticles encapsulated in a dielectric matrix have attracted sustained interest over several centuries owing to their unusual optical and electrical properties. Metal–dielectric nanocomposites show nonlinear and fast optical response near the SPR frequency owing to their enhanced third-order optical susceptibilities; thus, they have been applied in optical switching devices[1,2]. Nonlinear a.c. and d.c. electrical conductivities have also been observed in metal–dielectric percolating composites, wherein quantum tunnelling occurs between conducting particles near the percolation threshold[3,4]. Several approaches, such as the sol–gel process, metal–dielectric co-sputtering deposition, metal-ion implantation into a dielectric matrix and pulsed laser deposition, have been used to prepare metal–dielectric nanocomposites[5–8].

In addition to the aforementioned metal–dielectric nanocomposites that are mainly prepared in thin film or bulk forms, the one-dimensional noble-metal nanoparticle chain has become an intensive research focus because of its potential applications for nanoscale integrated optics below the diffraction limit of light[9,10]. It has been suggested theoretically and experimentally that the electromagnetic energy can be transported below the diffraction limit by a coupled-plasmon mode in the linear chains of noble-metal nanoparticles[9,10]. The successful synthesis of a one-dimensional hybrid nanosystem known as a 'peapod' offers a promising opportunity to realize a wide variety of functionalities[11,12]. The best-known example among them is the all-carbon hybrid peapod structure, consisting of fullerene molecules encapsulated in single-walled carbon nanotubes, which has been demonstrated to show several unusual physical properties[13,14]. In the present study, we put forward a microreactor approach for fabricating a self-organized metal nanoparticle chain encapsulated in a dielectric nanowire with SPR-induced conductivity therein.

Figure 1a shows a typical field-emission scanning-electron-microscopy (FESEM) image of the as-grown product taken at the edge of the substrate, in secondary-electron-image (SEI) mode. Well-aligned one-dimensional nanostructures can be seen clearly in this region and the nanowires have a typical length of 2–3 μm and a diameter of 40–60 nm. Figure 1b depicts the backscattered electron image (BEI) of the nanowires. Unlike the SEI, which gives mostly geometric contrast, the BEI reveals enhanced atomic contrast. Bright spots observed in the BEI indicate regions with elements of high atomic numbers. The high-magnification BEI of three individual nanowires is shown in the inset of Fig. 1b, confirming a hybrid peapod structure. It should be emphasized that the aligned nanowires were grown along the flow of gaseous species, and thus were predominantly observed at the downstream edge (0.5–0.6 mm) of the substrate. The sandwiched substrate assembly,

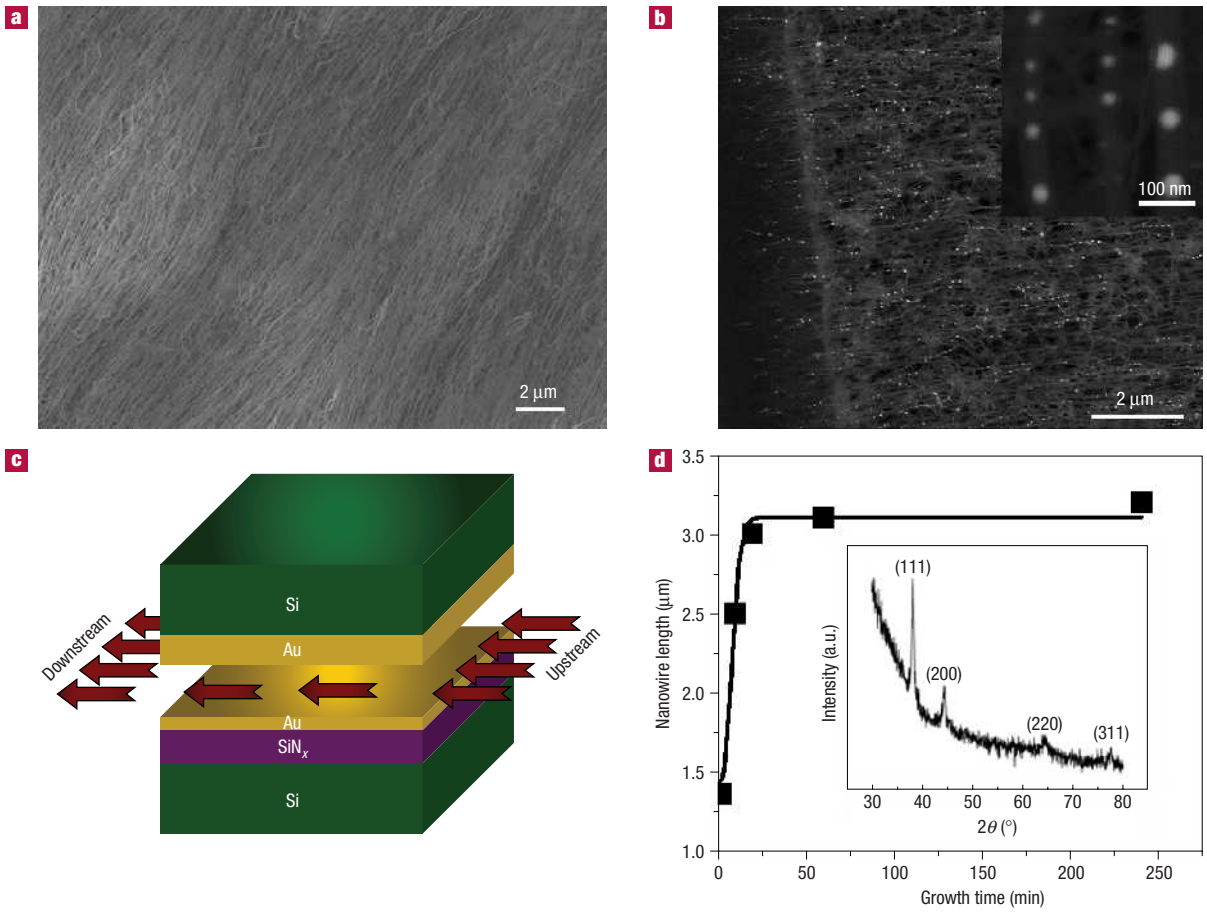

Figure 1 Growth and structure of the Au nanopeapodded silica nanowires. a, SEM image of well-aligned nanowires taken at the downstream edge of the substrate. **b**, BEI image of the nanowires. The inset shows the nanowires with a hybrid peapod structure. **c**, A schematic of the microreactor in a sandwich-like configuration. **d**, Nanowire length as a function of growth time. The inset presents the X-ray diffraction pattern of the composite nanowires (θ is the angle of reflection).

as shown schematically in Fig. 1c, functions as a microreactor for guiding the flowing stream of the gas phase. As illustrated in Fig. 1d, the length of the nanowires increased rapidly with growth time initially, and then saturated at around 20 min. The inset of Fig. 1d shows the X-ray diffraction pattern of the hybrid nanowires. All the diffraction peaks can be indexed to the characteristic peaks of gold without any trace of gold silicide.

The structural evolution of the hybrid nanowire was studied at different growth times (Fig. 2a–e). The chemical composition was examined using energy-dispersive X-ray (EDX) spectroscopy, which shows a gold core embedded in silica matrix without any trace of nitrogen (Fig. 2g,h). The copper lines in Fig. 2g and h were contributed from the copper grid that served as the sample support for transmission electron microscopy (TEM) analysis. An atomic ratio of Si/O = 1:0.6 was obtained on the nanowire sheath, indicating that the non-stoichiometric silica matrix is silicon-rich in nature. The structural evolution study suggests that the growth started with the formation of a hollow silica nanotube with a gold attachment at the end (Fig. 2a). Even though the formation of silicon-based nanotubes is commonly considered energetically unfavourable owing to high surface strain energy, it has also been adversely proposed that this surface strain can be minimized by hydrogen termination or by forming a monolayer of gold silicide on the inner surface of the tube[15,16]. Our process was carried out in hydrogen-rich plasma ambient, naturally giving rise to the hydrogen passivation of the silica nanotube. It should be pointed out that even though there was no detectable gold silicide in the X-ray diffraction, formation of a monolayer of silicide on the inner tube wall should not be excluded. With increasing growth time, gold started to flow into the hollow nanocavity (Fig. 2b) and showed a discrete wire-like morphology (Fig. 2c). The filling of gold in the nanocavity can be attributed to the capillary force, as was observed in other metal-filled silica nanotubes[17]. With prolonged growth, the discrete gold nanowires transformed into a droplet-like chain (Fig. 2d), owing to insufficient supply of gold, and finally evolved into a peapod (Fig. 2e), wherein crystalline gold nanoparticles (15–25 nm in diameter) with 50–100 nm interparticle distance were sheathed by the amorphous silica nanowire matrix.

It is worth mentioning that shrinkage in the nanocavity diameter between each gold droplet (that is, continuous filling of the tube with silica) was observed. More interestingly, the tube filling was accompanied by a slight shape deformation of the gold nanoparticles (Fig. 2f), suggesting the occurrence of compressive stress. A similar shape deformation has been reported in the megaelectronvolt ion-irradiated core–shell gold–silica colloids[18]. In our process, the source for the nanocavity filling can be attributed to the continuing supply of silicon-containing species from the top silicon cover during the nanowire growth. Possible oxygen sources may originate from residual oxygen of the chamber, native

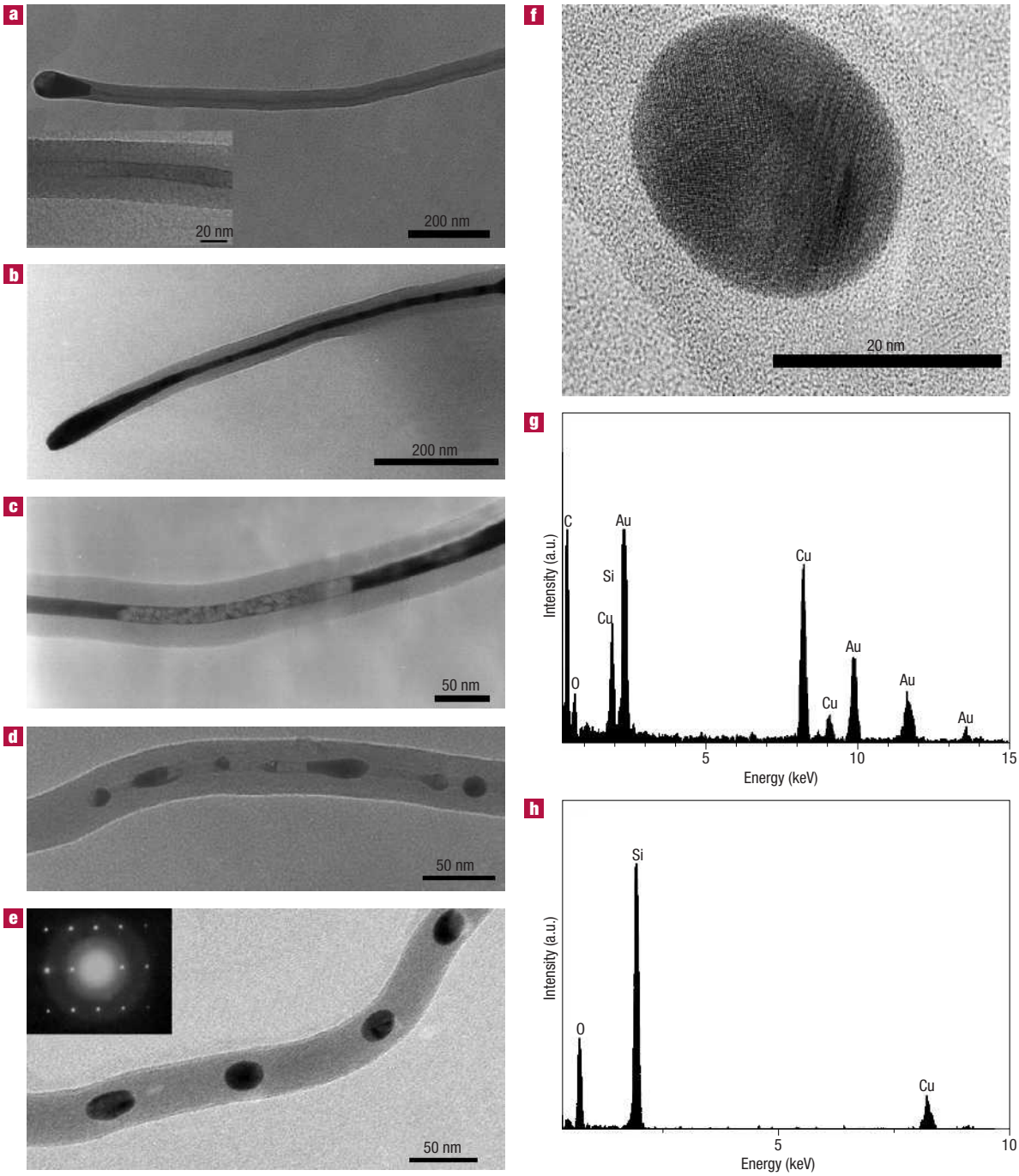

Figure 2 TEM images and EDX spectra of the gold nanopeapodded silica nanowire. a–e, TEM images showing structural evolution with growth times of **a**, 0 min, **b**, 2 min, **c**, 5 min, **d**, 10 min, and **e**, 20 min. The inset in **e** shows an electron-diffraction pattern recorded along the [120] zone axis. **f**, HRTEM image of the gold core in a silica nanowire, showing an ellipsoidal shape with an aspect ratio of ~1.18. **g–h**, EDX spectra of a composite nanowire taken at the shell and gold region, respectively.

oxide on the substrate and chemisorbed oxygen on the gold layer[19]. It has been reported that partial chemical reduction of SiO_2 will take place by breaking of the Si–O bonds when SiO_2 is attacked by the Au–Si eutectic above 500 °C (ref. 20). Both insufficient oxygen supply and the chemical reduction induced by the formation of the Au–Si eutectic may give rise to the structurally imperfect silica matrix and further facilitate silicon migration. It is worth noting that most nanoparticles show an anisotropic ellipsoidal shape with an aspect ratio of ~1.18 (Fig. 2f).

The high-resolution transmission electron microscopy (HRTEM) image (Fig. 2f) together with the selected-area electron-diffraction pattern (Fig. 2e inset) taken at the nanoparticle region can be well indexed to crystalline gold with a face-centred-cubic structure, which is in good agreement with the X-ray diffraction data (Fig. 1d inset).

Cathodoluminescence measurements on the gold nanopeapodded silica nanowires was carried out using a Gatan mono CL3 spectrometer in a JEOL JSM 6700F SEM system

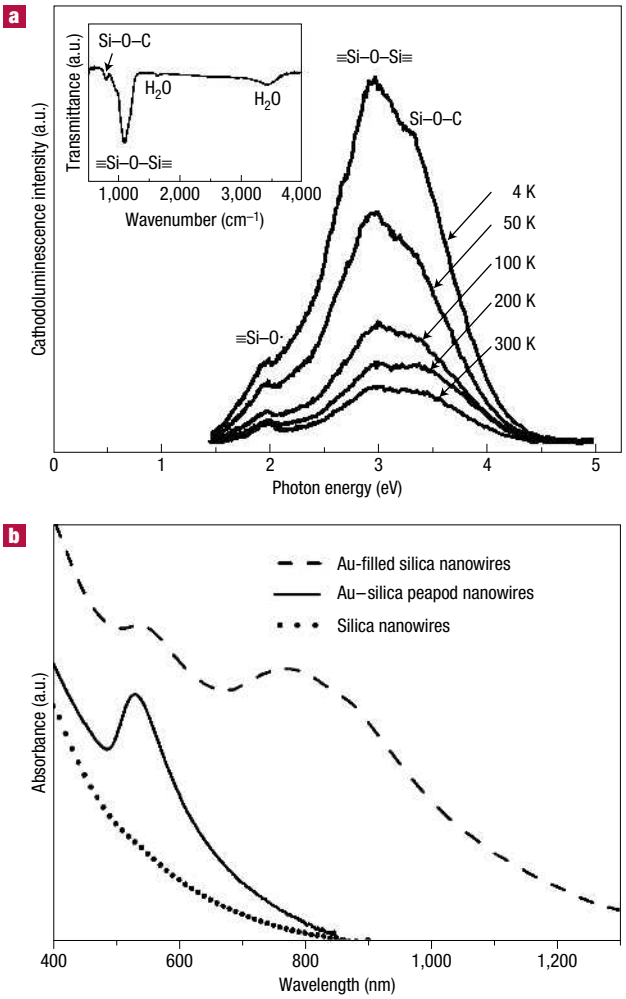

Figure 3 Cathodoluminescence spectra and ultraviolet–visible absorption spectra. a, Temperature-dependent cathodoluminescence spectra of gold nanopeapodded silica nanowires. The inset shows the corresponding FTIR spectrum. **b**, Optical absorption spectra for plain silica nanowires (dotted line), gold peapodded silica nanowires (solid line) and gold-filled silica nanowires wherein the aspect ratio of the gold segment is about 3–5 (dashed line).

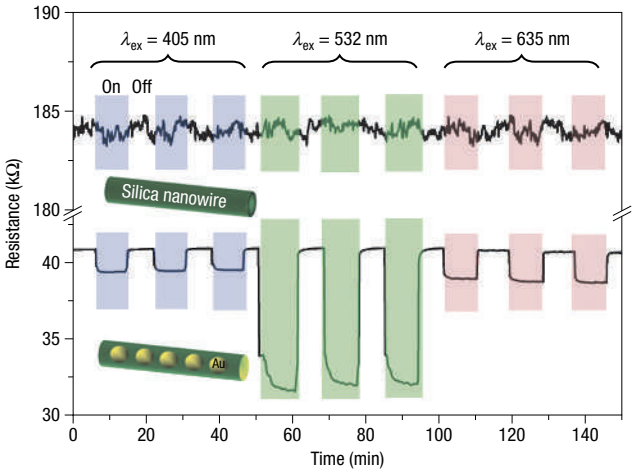

Figure 4 Photoresponse measurements. The room-temperature resistance response as a function of time to light illumination for plain silica nanowires (upper part) and gold nanopeapodded silica nanowires (lower part). Shaded (pink, excitation wavelength $\lambda_{ex} = 635$ nm; green, $\lambda_{ex} = 532$ nm; purple, $\lambda_{ex} = 405$ nm) and unshaded regions mark the light-on and light-off periods, respectively.

with an acceleration voltage of 8 keV. Figure 3a shows typical cathodoluminescence spectra of gold nanopeapodded silica nanowires at five different temperatures. The spectra are composed of three characteristic peaks at 3.3, 3.0 and 1.9 eV. The 1.9 eV band can be ascribed to the non-bridging oxygen hole centres or oxygen dangling bonds (≡Si–O); ref. 21. The 3.0 eV band corresponds to the twofold coordinated Si lone pair centres originating from the formation of strain bonds (≡Si–O–Si≡) when mechanical stress is applied to the silica glass[22,23]. The 3.3 eV band may be correlated with the formation of the Si–O–C owing to the reaction between ≡Si–O defects and carbon atoms during nanowire growth, which has been reported in carbon-doped silica[24,25]. As no carbon-containing gas reactants were intentionally introduced during nanowire growth, the incorporated carbon might originate from the sputtering process of gold thin films under ambient air, as confirmed by X-ray photoemission spectroscopy (not shown), or the residual contaminant in our reaction chamber. Analyses of bonding configurations from Fourier transform infrared (FTIR) data also confirm the existence of Si–O–C and ≡Si–O–Si≡ (Fig. 3a inset)[26]. Nevertheless, the FTIR data are obviously dominated by the ≡Si–O–Si≡ bonding signal, consistent with the cathodoluminescence data. The presence of this type of strained bond is clear evidence of the mechanical stress in the silica sheath, which may cause the shape deformation of gold nanoparticles inside the silica matrix.

Ultraviolet–visible absorption measurements were performed on a set of the composite nanowires grown on quartz substrate with different gold filling in the silica nanowires. The room-temperature ultraviolet–visible absorption spectra for plain silica nanowires (dotted line), gold-peapodded silica nanowires (solid line) and gold-filled silica nanowires wherein the gold segments show an aspect ratio of 3–5 (dashed line) are shown in Fig. 3b. The gold-filled and gold-peapodded silica nanowires reveal a pronounced SPR absorption band at 532 nm, whereas the plain silica nanowires do not show any SPR absorption. The SPR band at 532 nm is attributed to the transverse plasmon mode and the longer wavelength band is associated with the longitudinal plasmon mode[27], which was observed for composite nanowires containing gold segments of high aspect ratio (see the dashed line in Fig. 3b and Supplementary Information, Fig. S1). The absence of the longitudinal mode in the gold-peapodded nanowires (see the solid line in Fig. 3b) may be ascribed to the small aspect ratio (<1.2) of the gold nanoparticles[27]. The observed background in the composite nanowires originates from an interband transition of valence electrons in the *d* band to the Fermi surface[28].

Photoresponse measurements based on the nanowire ensemble devices were conducted under alternate light illumination of different wavelengths and under dark conditions. Before the experiment, the background resistance based on a blank substrate (SiN-coated Si(100)) under light illumination (635, 532 and 405 nm) was also investigated as a reference. The background resistance from the blank substrate showed very high resistance up to 15 GΩ and no photoresponse was observed on light illumination. As shown in Fig. 4, the plain silica nanowire device shows high resistance (184 kΩ) with no apparent fluctuation on light illumination. Note that this value is approximately five orders smaller compared with the blank SiN_x-coated Si substrate. The incorporation of carbon in the silica nanowires, as

indicated from the cathodoluminescence and FTIR data mentioned above, might account for the marked decrease in resistance. Possible conduction mechanisms including electron hopping, Schottky emission, Poole–Frenkel emission and Fowler–Nordheim tunnelling are suggested to interpret the electrical conduction in carbon-doped silicon oxide[29]. The resistance of the hybrid peapod nanowire device shows nearly a five times smaller value than its counterpart without the gold nanoparticles. More interestingly, the hybrid peapod nanowire device presents a wavelength-dependent photoresponse in resistance. The photoresponse behaviour at a SPR wavelength of 532 nm shows a larger difference in resistance between the illumination on and off conditions (Fig. 4). The resistance change is nearly five times that observed using 632 and 405 nm light. Furthermore, an excitation-intensity-dependent resistance was measured using 532 nm light at various pumping powers (see Supplementary Information, Fig. S2). It is believed that the enhanced photosensitive behaviour observed from the hybrid nanowire device can be attributed to the SPR, as the hybrid nanowires have a pronounced SPR absorption at 532 nm. The enhancement of photoresponse behaviours arising from the excitation of the surface plasmon has been reported for metal–oxide–metal (MOM) tunnelling junctions, which is attributed to the generation of hot electrons owing to the decay of surface plasmon polaritons[30]. The generated hot electrons drift or diffuse to the oxide barrier and tunnel to the counterelectrode. In our case, one-dimensional gold nanopeapodded silica nanowire can be regarded as an MOM tunnelling junction in series. Generation of hot electrons and electron tunnelling through the oxide nanowires may contribute to the enhanced photoresponse behaviour in our hybrid nanowire.

Applicability of the present method to other hybrid nanowires has also been verified (for example, see Supplementary Information, Fig. S3). The microreactor technique offers the advantage of forming a dielectric-based hollow tubular nanostructure followed by a filling of the metal core in a self-organized manner. We believe that this simple one-step approach could be extended to the preparation of other metal–dielectric peapod-type nanowires with different functionalities.

METHODS

HYBRID NANOWIRE SYNTHESIS

Fabrication of gold-peapodded silica nanowires was carried out in an AsTex 5 kW microwave chamber. A thin gold layer (~7 nm), serving as a catalytic layer, was deposited on the SiN_x-coated Si(100) substrate (10 mm × 10 mm) using a sputtering technique. A separate gold-coated (28−112 nm) Si wafer was placed (face down) on top of the Au/SiN_x-coated Si(100) substrate in a sandwich configuration, which was then transferred into the reaction chamber. The growth of one-dimensional composite nanowires was carried out in two stages. First, H_2 (99.999%) was introduced into the chamber to generate H_2 plasma for the formation of catalytic gold nanoparticles on the SiN_x-coated Si(100) substrate at 40 torr for 1 min, while the microwave power was fixed at 1,500 W. For the second stage, a gas mixture of H_2 (200–250 s.c.c.m.) and NH_3 (300–350 s.c.c.m.) was introduced into the chamber. The chamber pressure was maintained at 50–70 torr and the microwave power was kept at 1,500 W for 20 min during growth. The substrate temperature was 530 °C measured by an optical pyrometer (CHINO IR-H) through a quartz window.

CHARACTERIZATION

Observation of the surface morphology of the nanowires was conducted using FESEM (JEOL 6700) in both the secondary and back-scattered imaging modes. X-ray diffraction (Rigaku, D/Max-RC) and HRTEM (JEOL JEM-4000EX) were used to investigate the microstructure of the composite nanowires. FTIR spectra were measured with a Jasco FT/IR-480 Plus spectrometer from 400 to 4,000 cm^{-1}. Cathodoluminescence studies were carried out using a Gatan mono CL3 spectrometer in the FESEM system. Ultraviolet–visible absorption spectra were recorded using a Hitachi U-3310 spectrophotometer at room temperature. Photoresponse measurement was performed using an ensemble of hybrid nanowires grown on a SiN_x-coated Si substrate under an ambient pressure of 10^{-6} torr at room temperature. Two electrodes separated by 5 mm were fabricated by applying silver glue at the two ends of the hybrid nanowire ensemble device. The voltage of the d.c. source was maintained at 10 V and the current was measured by a picoammeter (Keithley 237). Three different light sources including the continuous-wave beam of a diode laser (10 mW; 405 nm), a green solid-state laser (10 mW; 532 nm) and a red He–Ne laser (10 mW; 632 nm) were used to test the photoresponse behaviour of the nanowire ensemble devices.

Received 20 August 2005; accepted 9 November 2005; published 22 January 2006.

References

1. Hache, F., Ricard, D. & Flytzanis, C. Optical nonlinearities of small metal particles: surface-mediated resonance and quantum size effects. *J. Opt. Soc. Am. B* **3,** 1647–1655 (1986).
2. Haglund, R. F. *et al.* Picosecond nonlinear optical response of a Cu:silica nanocluster composite. *Opt. Lett.* **18,** 373–375 (1993).
3. Kiesow, A., Morris, J. E., Radehaus, C. & Heilmann, A. Switching behavior of plasma polymer films containing silver nanoparticles. *J. Appl. Phys.* **94,** 6988–6990 (2003).
4. Liao, H. B. *et al.* Large third-order optical nonlinearity in Au:SiO_2 composite films near the percolation threshold. *Appl. Phys. Lett.* **70,** 1–3 (1997).
5. Wang, W. T. *et al.* Resonant absorption quenching and enhancement of optical nonlinearity in Au:$BaTiO_3$ composite films by adding Fe nanoclusters. *Appl. Phys. Lett.* **83,** 1983–1985 (2003).
6. Dalacu, D. & Martinu, L. Temperature dependence of the surface plasmon resonance of Au/SiO_2 nanocomposite films. *Appl. Phys. Lett.* **77,** 4283–4285 (2000).
7. Pardo-Yissar, V., Gabai, R., Shipway, A. N., Bourenko, T. & Willner, I. Gold nanoparticle/hydrogel composites with solvent-switchable electronic properties. *Adv. Mater.* **13,** 1320–1323 (2001).
8. Dhara, S. *et al.* Quasiquenching size effects in gold nanoclusters embedded in silica matrix. *Chem. Phys. Lett.* **370,** 254–260 (2003).
9. Quinten, M., Leitner, A., Krenn, J. R. & Aussengg, F. R. Electromagnetic energy transport via linear chains of silver nanoparticles. *Opt. Lett.* **23,** 1331–1333 (1998).
10. Brongersma, M. L., Hartman, J. W. & Atwater, H. A. Electromagnetic energy transfer and switching in nanoparticle chain arrays below the diffraction limit. *Phys. Rev. B* **62,** R16356–16359 (2000).
11. Smith, B. W., Monthioux, M. & Luzzi, D. E. Encapsulated C_{60} in carbon nanotubes. *Nature* **396,** 323–324 (1998).
12. Wu, J. S. *et al.* Growth and optical properties of self-organized Au_2Si nanospheres pea-podded in a silicon oxide nanowire. *Adv. Mater.* **14,** 1847–1850 (2002).
13. Yoon, Y.-G., Mazzoni, M. S. C. & Louie, S. G. Quantum conductance of carbon nanotube peapods. *Appl. Phys. Lett.* **83,** 5217–5219 (2003).
14. Chiu, P. W. *et al.* Temperature-induced change from p to n conduction in metallofullerene nanotube peapods. *Appl. Phys. Lett.* **70,** 3845–3847 (2001).
15. Seifert, G., Köhler, Th., Urbassek, H. M., Hernández, E. & Frauenheim, Th. Tubular structures of silicon. *Phys. Rev. B* **63,** 193409 (2001).
16. Leeuw, N. H. d., Du, Z., Li, J., Yip, S. & Zhu, T. Computer modeling study of the effect of hydration on the stability of a silica nanotube. *Nano Lett.* **3,** 1347–1352 (2003).
17. Li, Y., Bando, Y. & Golberg, D. Indium-assisted growth of aligned ultra-long silica nanotubes. *Adv. Mater.* **16,** 37–40 (2004).
18. Roorda, S. *et al.* Aligned gold nanorods in silica made by ion irradiation of core-shell colloidal particles. *Adv. Mater.* **16,** 235–237 (2004).
19. Franceschetti, A., Pennycook, S. J. & Pantelides, S. T. Oxygen chemisorption on Au nanoparticles. *Chem. Phys. Lett.* **374,** 471–475 (2003).
20. Alessandrini, E. I., Campbell, D. R. & Tu, K. N. Interfacial reaction in MOS structures. *J. Vac. Sci. Technol.* **13,** 55–57 (1976).
21. Yao, B., Shi, H., Zhang, X. & Zhang, L. Ultraviolet photoluminescence from nonbridging oxygen hole centers in porous silica. *Appl. Phys. Lett.* **78,** 174–176 (2001).
22. Munekuni, S. *et al.* Si-O-Si strained bond and paramagnetic defect centers induced by mechanical fracturing in amorphous SiO_2. *J. Appl. Phys.* **70,** 5054–5062 (1991).
23. Yu, D. P. *et al.* Amorphous silica nanowires: Intensive blue light emitters. *Appl. Phys. Lett.* **73,** 3076–3078 (1998).
24. He, H., Wang, Y. & Tang, H. Intense ultraviolet and green photoluminescence from sol–gel derived silica containing hydrogenated carbon. *J. Phys. Condens. Matter* **14,** 11867–11874 (2002).
25. Zhao, J. *et al.* Intense short-wavelength photoluminescence from thermal SiO_2 films co-implanted with Si and C ions. *Appl. Phys. Lett.* **73,** 1838–1840 (1998).
26. Socrates, G. *Infrared Characteristic Group Frequencies* (Wiley, Bristol, 1980).
27. Jana, N. R., Gearheart, L. & Murphy, C. J. Seed-mediated growth approach for shape-controlled synthesis of spheroidal and rod-like gold nanoparticles using a surfactant template. *Adv. Mater.* **13,** 1389–1393 (2003).
28. Gu, J.-L. *et al.* Incorporation of highly dispersed gold nanoparticles into the pore channels of mesoporous silica thin films and their ultrafast nonlinear optical response. *Adv. Mater.* **17,** 557–560 (2005).
29. Yiang, K. Y., Yoo, W. J., Guo, Q. & Krishnamoorthy, A. Investigation of electrical conduction in carbon-doped silicon oxide using a voltage ramp method. *Appl. Phys. Lett.* **83,** 524–526 (2003).
30. Berthold, K., Höpfel, R. A. & Gornik, E. Surface plasmon polariton enhanced photoconductivity of tunnel junctions in the visible. *Appl. Phys. Lett.* **46,** 626–628 (1985).

Acknowledgements

This research was financially supported by the Ministry of Education and National Science Council in Taiwan. Technical support provided by the Core Facilities for Nano Science and Technology in Academia Sinica and National Taiwan University are acknowledged. Fruitful discussions and technical help from Y. F. Huang, S. Chattopadhyay, as well as C.-H. Chen, J.-S. Hwang and R.-l. Chang were also appreciated.

Correspondence and requests for materials should be addressed to L.-C.C.

Supplementary Information accompanies this paper on www.nature.com/naturematerials.

Competing financial interests

The authors declare that they have no competing financial interests.